Quantification of Advective Transport Phenomena to Better Understand Dispersion in the Field

by Willem J. de Lange

Abstract

Observation of dispersion in field situations has left three issues that may be better understood by applying advective transport phenomena. (1) In some experiments, the longitudinal dispersivity becomes constant with increasing pathlength and in other cases it remains growing. (2) Dispersivities reported from multiple comprehensive observations at a single site differ at similar pathlength in some cases more than a factor two. (3) The observed difference between the plume fronts and plume tails is not represented in the reported parameters. The analytic equations for advective transport phenomena at macroscale of De Lange (2020) describe the thickness of the affected flow-tube and the spread of the plume front and tail. The scale factor defines the size of the averaging domain and so of the initial phase. The new macroscale correlation coefficient relates the growth of the longitudinal dispersivity beyond the initial phase to the aquifer heterogeneity. Using stochastic parameters for the aquifer heterogeneity, the parameters are quantified at 14 field experiments in the United States, Canada and Europe enabling the comparison of calculated and reported final dispersivities. Using the quantified parameters, 146 reported and calculated dispersivities along the traveled paths show a good match. A dispersivity derived from the local plume growth may differ a factor of two from the aquifer-representative value. The growths of plume fronts and tails between two plume stages are assessed in 14 cases and compared to calculated values. Distinctive parameters for the plume front and tail support better understanding of field situations. A user-ready spreadsheet is provided.

Introduction

Observation of dispersion in field situations has left three issues that may be better understood by applying advective transport phenomena: (1) In some experiments the longitudinal dispersivity becomes constant with increasing pathlength and in other cases it remains growing. (2) Dispersivities reported from multiple comprehensive observations at a single site differ for similar pathlength, in some cases more than a factor 2. (3) The observed difference between the lengths of the front and

Unit Subsurface and Groundwater Systems, Deltares, P.O. Box 85467, 3508 AL, Utrecht, The Netherlands; wim.delange@deltares.nl

the tail of a plume is not represented in the parameters reported from field experiments.

Recent studies of the relation between longitudinal dispersivity and travel distance have led to theoretical understanding (Neuman and Tartakovsky 2009; Fiori et al. 2017) and analyses of reported data (Gelhar et al. 1992; Schulze-Makuch 2005). Zech et al. (2015) concluded that their selected data does not support a unique scaling law relationship between the longitudinal dispersivity and travel distance or scale. This conclusion is supported by comprehensive field experiments carried out at Twin Lakes (Moltyaner and Killey 1988), Borden (Rajaram and Gelhar 1991), and Cape Cod 1 (Hess et al. 2002) that show a constant or equilibrium dispersivity with increasing travel distance while other experiments at Krauthausen (Vereecken et al. 2000), Wagna (Fank and Rock 2005), and MADE (Adams and Gelhar 1992) show a permanent growth or nonequilibrium dispersivity. At Cape Cod (Hess et al. 2002), the dispersivity reported for the second experiment is twice that reported for the first experiment at about half of the travel distance.

Field experiments report longitudinal dispersion in terms of the overall parameters, dispersivity and/or variance, thus ignoring the difference between the front and tail of the plume. At micro-scale, asymmetric dispersion
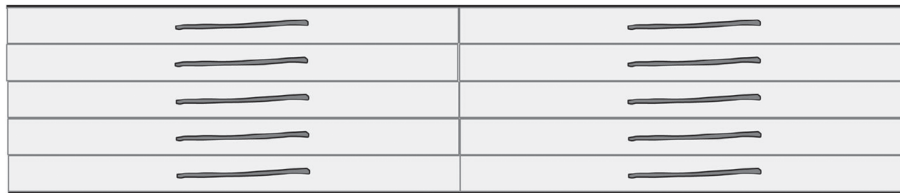
Figure 1. Vertical cross section: Periodic domains filling up an aquifer (from De Lange 2020).

has been explained and simulated (Feehley et al. 2000) by diffusion-limited mass transfer between the flowing and nearly stagnant groundwater in pores or low conductivity zones. At macroscale, the asymmetry of the plume dispersion has been simulated by Janković et al. (2006) using three-dimensional, Darcian flow through many, arbitrarily placed spherical inclusions of fixed size with conductivities varying according to a stochastic distribution. For this concept (Fiori et al. 2006) presented an approximate semi-analytical solution. Flow through two-dimensional inclusions has led to analytical equations for dispersivity in the works of Eames and Bush (1999), Dagan and Lessoff (2001) and Lessoff and Dagan (2001). In line with the latter research but derived independently, the analytic equations of De Lange (2020) describe asymmetric dispersion at macroscale by advective transport phenomena in two-dimensional vertical space.

The present aim is to support better understanding of the growth of dispersion observed in field observations by offering a practical tool for the spread and dispersivity of plume fronts and plume tails. The results from this tool are compared with those reported for 14 well-documented extensive field experiments at nine sites in the United States, Canada, and Europe.

The dispersion parameter for modeling presented in De Lange (2020) is different from the dispersivity derived from field situations. The application in numerical simulations requires extensive analysis that is beyond the present scope. This will be reported in the future.

The present work is limited to longitudinal dispersion on macroscale in a granular aquifer with ambient flow. Forced flow and fissures as included the work of Neuman (1990) are excluded because the analytic equations of De Lange (2020) do not apply to radial and non-Darcian flow. Also, excluded are transient effects, being one of the causes of horizontal transverse dispersion, or diffusion, being relevant at low velocities and one of the causes of vertical transverse dispersion.

The conceptual model is illustrated by flow and equipotential lines in a vertical cross-section generated with the analytic element method (Strack 1989) using line-doublets for the boundary of the conductivity zone and line-dipoles for the aquifer boundary at top and bottom as well as for the line-shaped conductivity zones in Figure 4.

Methodology

The first part of the description of the methodology below continues on the previous work (De Lange 2020), in which the Equations 1–7 have been derived. The second part describes an extension of the methodology and is explicitly mentioned in the text.

Conceptually, the aquifer is subdivided (Figure 1) in domains of the same size each containing a discrete elongated zone with a contrasting conductivity of which the properties are derived from stochastic parameters (Figure 2). Dispersion is conceptualized (Figure 3) as the change of flow of a front entering on the upstream side of the domain into the dispersed front at the downstream side, which is entirely due to the nonuniform velocity field caused by the zone with the contrasting conductivity. This inner-domain process is repeated in subsequent domains (Figure 4) causing the overall dispersion over longer distances and times.

Dispersion in an aquifer is conceptualized as stacked, repeated domains A with a conductivity zone (Figure 1), in each of which the process is completed once. Although the idea of repetition of the dispersion process was developed independently, it is similar to the concept of periodicity used in the different theory by Eames and Bush (1999).

The properties of the conductivity zone were derived from the classic stochastic parameters (Gelhar 1993) describing the aquifer heterogeneity. The characteristic length λ represents the local correlation distance around an observation point (Figure 2). The length and thickness of the zone of correlation equals twice the horizontal (index h) and vertical (index v) characteristic length $2\lambda_h$ and $2\lambda_v$ (L) respectively. The length L_A and thickness D_A of a domain A relate to the characteristic lengths by the scale factor N according to $L_A = 2\lambda_h/N$ and $D_A = 2\lambda_v/N$, so a factor $1/N$ tot the size of the conductivity zone. The lognormal distribution of the conductivity k describes the average k_a in the background aquifer and a characteristic high and low value at the standard deviation. A high
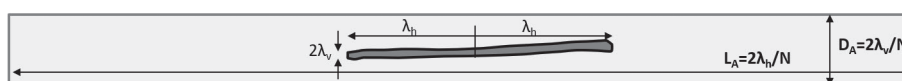

Figure 2. Vertical cross section: Size of domain A and conductivity zone related to characteristic lengths.
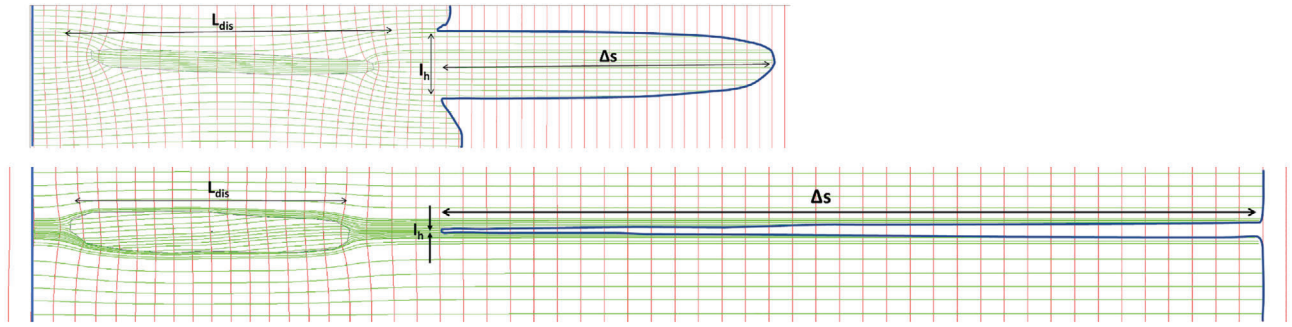
Figure 3. Vertical cross section (red lines are equipotentials, green lines path lines end at the same travel time): A straight front of water particles (at left) is changed after passing through a zone with a conductivity five times higher (top) and lower (bottom) than that of the background of the aquifer. Blue lines indicate the initial and the final shape of the front.

conductivity zone adds spread to the front of a plume while a low conductivity inclusion adds spread to the tail of a plume The conductivity ratios for the front $\kappa_f = k_a/k_f$ and tail $\kappa_t = k_a/k_t$ can be calculated from the log-conductivity variance by:

$$1/\kappa_f = \kappa_t = e^{\sqrt{\sigma^2_{lnk}}} \qquad (1)$$

Figure 3, top shows the growth of a plume front by flowing through a high conductivity zone in a uniform flow field. A part of the path lines (green) in the aquifer show convergence while entering the zone (left in Figure 3, top). Inside the zone, the water particles travel with increased velocity (dense path lines) while the water particles outside the zone travel slower. The path lines leaving the zone spread out (right in Figure 3, top) and the water particles are clearly ahead of the ones aside of the zone. Figure 3, bottom shows the impact of a low conductivity zone. The plume tail develops in backward direction relative to the average movement of the water particles. Only a few path lines or water particles enter the zone and generate a thin tail with a length of more than twice that of the front. In conclusion, a high-conductivity zone generates convergence and spread out of path lines over a thick wake forming the front (Figure 3, top) and a low-conductivity zone affects the path lines over a thin wake forming the tail (Figure 3, bottom). Both spreads in the water particle distribution occur at the same time in a domain A, because a domain A represents the complete variation of the conductivity characterized by the conductivity ratios for the front and tail of the plume.

The plume in Figure 3 is described by (1) the spread $\Delta s_{A,j}$ (L), in which index A indicates domain A, in which index j equals for f the front and t for the tail of the plume, and (2) the plume thickness W_p (L) called the wake after (Eames and Bush 1999) who, however, did not present an equation for it. In Figure 3, the so-called length of distortion L_{dis} (L) is the length over which the velocity is clearly not uniform over the thickness. The red lines in Figure 3 show that the potential or hydraulic head is virtually constant in vertical direction across much of the two conductivity zones. Neglecting the zones of

convergence and spread out, the gradient in the potential in the flow direction is essentially equal inside and outside each conductivity zone. Then, the following equations hold (De Lange 2020):

$$\Delta s_{A,j} = \left(1 - \kappa_j/\eta_j\right) L_{dis,j} \qquad (2)$$

$$W_{p,j} = D_A/\left(1 + \kappa_j(1/N - 1)\right) \qquad (3)$$

In which $\kappa_j = k_a/k_j$ (−) is de conductivity ratio and $\eta_j = n_a/n_j$ (−) is the porosity ratio. In Figure 3, a single value of $\sigma^2_{\ln k}$ of 2.6 is used causing in the elongated zone a factor 5 higher as well as lower conductivity than that of the aquifer. It follows from the term $(1 - \kappa_j/\eta_j)$ in Equation 2 that the spread $\Delta s_{A,f}$ for the front ($\kappa \ll 1$) is limited to $L_{dis,f}$, whereas the spread $\Delta s_{A,t}$ for the tail ($\kappa \gg 1$) is negative (relative to the traveled distance) and limited only to the traveled path length S. The length of distortion L_{dis} (L) extends the length of the conductivity zone by about the lengths of the areas with contracting and diverging path lines at both ends of the conductivity zone (De Lange 2020), which are about equal to the wake $W_{p,j}$ and different for the front and tail of the plume:

$$L_{dis,j} = 2\left(\lambda_h + W_{p,j}\right) \qquad (4)$$

Equations 2–4 may also be applied to the case of a single zone in an aquifer with both conductivities known. In the present methodology, the parameters are assumed to be stochastic-based as described above.

In each domain A so for $S < L_A$, the dispersion process is averaged leading to linear growth of the plume with travel distance S (L). This linear growth is often observed in the initial phase in field experiments.

$$\Delta s_j(S) = \Delta s_{A,j} * S/L_A \text{ for } S < L_A \qquad (5)$$

The growth of the variance with the path length determines the dispersivity by the well-known (e.g., Appelo and Postma 1993) equation:

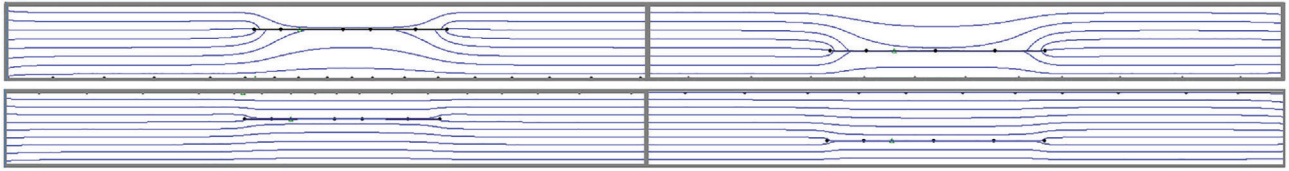$$\alpha_j = \Delta s_j(S)^2/2S \qquad (6)$$

Figure 4. Vertical cross section (blue line = streamline): Water particles flowing through elongated strongly (top) and hardly (bottom) increased conductivity zones relative to the aquifer average causing dependent (top) and independent (bottom) repetition of dispersion (see text).

The analysis in De Lange (2020) has shown that the variance of the total plume can be interpreted as the product of the standard deviations or the spreads of the front and the tail, so $\Delta s_{plume}^2 = \Delta s_f * \Delta s_t = \sqrt{\left(\Delta s_f^2 * \Delta s_t^2\right)}$. Division by $2S$ and use of Equation 6 leads to:

$$\alpha_{plume} = \sqrt{\left(\alpha_f * \alpha_t\right)} \qquad (7)$$

which describes that the dispersivity of the total plume α_{plume} is the geometric average of the dispersivities of the front and tail.

Next, the description by De Lange (2020) will be extended for multiple, repeated domains so for cases in which the traveled distance S is larger than the length of a domain A. The process of repetition can be described as follows. In the first domain A (gray box at left in Figure 4, top) containing a long zone with high-conductivity, fast water particles in the plume front generate a thick wake. In the next domain A (gray box at right in Figure 4, top), it is likely that most water particles will be within the thick wake and again become fast, so determine the plume front. Then, the spread in the plume front adds up in both domains. This here-called dependently repeated dispersion is believed to generally occur in heterogeneous aquifers. In weakly heterogeneous aquifers containing zones with a slightly different conductivity, the wake is about equal to the thickness of this zone. Because the conductivity zones vary in vertical position (Figure 4, bottom), water particles become relatively fast or slow independently of what occurred in the previous domain A. This here-called independently repeated dispersion describes that the spread of the front does not add up in subsequent domains A. It is characterized by a constant dispersivity and a linear growth of the variance of the particle distribution with travel distance.

The distinction between dependently and independently repeated dispersion leads to the following. In stochastic theory, the combination of normal distributions is described in terms of summation of average values and standard deviations (Sachs 1984, 77–78). The standard deviations are added up (index 1 and 2) according to:

$$\Delta s = \sqrt{\Delta s_1^2 + \Delta s_2^2 + 2r\,\Delta s_1 * \Delta s_2} \qquad (8)$$

The correlation coefficient in the cross-product r ($0 \leq r \leq 1$) represents the interdependency of the two stochastic distributions. In groundwater, the parameter r is called the macroscale dispersion correlation coefficient which describes the interdependency of dispersion occurring in the subsequent domains A. For $r = 0$, Equation 8 becomes $\Delta s_{sum}^2 = \sum \Delta s_i^2$ so variances add up which represent independent repeated dispersion. For $r = 1$, the summation becomes $\Delta s_{1+2} = \sqrt{\left(\Delta s_1^2 + \Delta s_2^2 + 2\Delta s_1 \Delta s_2\right)} = \sqrt{\left(\Delta s_1 + \Delta s_2\right)^2} = \Delta s_1 + \Delta s_2$ so standard deviations add up representing dependent repeated dispersion. Values of r between 0 and 1 represent intermediate dependency. Equation 8 can be expanded for more than two domains A by writing out $\Delta s_{sum} = \sqrt{\left(\Delta s_1 + \Delta s_2 + \Delta s_3 + \cdots\right)^2}$ and adding r to all cross-products. In each domain A, the standard deviation Δs_i ($i = 1, 2, 3, \ldots$) equals Δs_A. With $p = S/L_A$ called the repetition ratio for the path length S, this leads to:

$$\Delta s_{S,f} = \Delta s_{A,f}\sqrt{\left(p((p-1)r+1)\right)} \text{ for } S > L_A \qquad (9)$$

In the application to field experiments, p is considered a continuous parameter. For $r = 1$, Equation 9 becomes $\Delta s_{S,f} = \Delta s_{A,f}\,p$. Using Equation 6, the front dispersivity over the path length S becomes $\alpha_{S,f} = \Delta s_f^2/2S$ and the dispersivity in a single domain A over the length L_A becomes $\alpha_{A,f} = \Delta s_{A,f}^2/2L_A$. Combination of these three equations leads to $\alpha_{S,f} = \alpha_{A,f}\,p$ expressing the linear growth of the front dispersivity with path length. Similarly, $r = 0$ leads to $\alpha_{S,f} = \alpha_{A,f}$ generating a constant front dispersivity with path length. In weakly heterogeneous aquifers ($r = 0$), the plume growth is nearly symmetrical. In strongly heterogeneous aquifers ($r = 1$), a part of the tracer remains in low conductivity zones near the injection point causing the plume tail to grow linear with travel distance, which is similar to the growth of the plume front. So, the plume tail and the plume front develop in about the same way with respect to the aquifer heterogeneity, but with different lengths.

The dispersivity resulting from the above equations is site-specific for all parameters except the path length that is case-specific or depending on the stage of development of the plume. Appendix A describes the steps in the calculation of dispersivities in the user-ready spreadsheet in File S1, Supporting Information.

Table 1
Categories of Data Assessment

Category	Data Origin
Estimated	Based on similar, described situation; no direct source available
Interpreted	Value translated from graph, distribution, figure in reference
Deduced	Determined based on multiple references
Calculated	Calculated from data in reference
From	As reported in reference

Assessing Parameters Values from Field Experiments

Any application starts with the assessment of parameter values. Fourteen field experiments at nine sites in the United States, Canada and Europe were selected on the availability of information of the stochastic parameters describing the aquifer and on the development of the plume along the traveled length in terms of dispersivities.

Reported Parameter Values

The stochastic aquifer parameters λ_h, λ_v, $\sigma_{\ln k}^2$ and the aquifer thickness D_a at the nine sites have been derived in different ways using different types of sources and are classified in five categories (see Table 1). Table 2 presents for each site the results and nick-names used throughout the present work and ordered with increasing aquifer heterogeneity. Most of the input data has been reported explicitly, so comes from the original source. Some input data could be calculated directly from published data. For two cases in Germany, input data has been deduced from multiple sources. Most aquifer thicknesses have been interpreted from pictures. In the Wagna case, the river bed aquifer has been estimated to be similarly heterogeneous as the aquifer in Krauthausen. The range in $\sigma_{\ln k}^2$ is more than two orders of magnitude. The ratios of λ_h and λ_v differ up to a factor 25. In Table S.3.1 in File S3, the origin per parameter is specified in detail.

The porosity ratio η determines the spread Δs as part of the ratio κ/η in Equation 2 and can be used to analyze the impact of a single zone on the spread. Local porosity variation may affect local flow velocity and may explain variation in the dispersivity based on breakthrough curve interpretation (e.g., Horkheim; Ptak and Teutsch 1994). To use field data in the present work, the distribution of the variation of the quotient k/n in the aquifer is needed. Average effective porosities have been reported for Borden (Sudicky 1986), Cape Cod (Garabedian et al. 1992), and Denmark (Jensen et al. 1993). Vereecken et al. (2000) and Table 1) report statistics of the bulk porosity at Krauthausen. At present, the variation of k/n at the scale of the aquifer is not known and requires further research. Following common practice of Jankovic et al. (2003) and Fiori et al. (2013) the effective porosity is taken constant, so $\eta = 1$.

Parameters Assessed from Final Dispersivities

The parameters N and r will be assessed from comparison of calculated and reported final dispersivities α_{final} (so different to the dispersivities observed along the plume path used in the application to field experiments) for the 14 field experiments. Table 3 shows these reported final values that are assumed to represent the dispersion in the experiment as completely as possible. All cases (field experiments) have been reviewed by Zech et al. (2015), except the case at Wagna. Multiple experiments at a single site provide independent values at varying travel distances and significantly add to the assessment of the site-specific parameters N and r as will be shown below.

At *Cape Cod 2*, the dispersivity at the largest travel distance was calculated using Equation 6, see section Application to individual field experiments. At *Borden 2*, the multiplication by a factor 2–4 as suggested in Gelhar et al. (1992) was applied. At *Krauthausen*, the dispersivity derived from second moment of the tracer distribution is based on the latest complete plume shape, which is before a significant part of the plume had traveled beyond the reach of the observation system. At *Sued*, the plume also moved out of the observation network. However, the dispersivity in the final stage is not affected by the unknown plume shape, because it comes from breakthrough curve interpretation. At *Horkheim* (Ptak and Teutsch 1994, Table 7), the dispersivity comes from the

Table 2
Site-specific Parameter Values ($\sigma_{\ln k}^2$ = log conductivity variance, λ_v, λ_h = vertical, horizontal characteristic length, D_a = aquifer thickness)

Site Nickname	Primary Reference	$\sigma_{\ln k}^2$	λ_v (m)	λ_h (m)	D_a (m)
Twin Lakes	Moltyaner and Killey (1988)	**0.04**	**0.5**	**20**	*12*
Cape Cod	Garabedian et al. (1992)	**0.24**	**0.39**	**8**	**30**
Denmark	Jensen et al. (1993)	**0.37**	*0.1*	**2.5**	*5*
Borden	Sudicky et al. (1983)	**0.38**	**0.12**	**2.8**	**8**
Krauthausen	Vereecken et al. (2000)	**1.08**	**0.37**	**6.66**	*7*
Wagna	Fank and Rock (2005)	1.08	*0.15*	11	**4**
Sued	Boesel et al. (2000)	**2.13**	**2**	**60**	*5*
Horkheim	Ptak and Teutsch (1994)	**2.34**	0.15	**25**	**3**
MADE	Adams and Gelhar (1992)	**7.00**	**1.5**	**12.3**	**10.0**

Table 3
Final Dispersivities α_{final} with Travel Distances S from Field Experiments

Experiment	S (m)	α (m)	Dispersivity Value from
Twin Lakes 1	40	0.04–0.16	Moltyaner and Killey (1988)
Twin Lakes 2	266	0.55	Moltyaner et al. (1993)
Cape Cod 1	200	0.96	Garabedian et al. (1992)
Cape Cod 2	41	1.22[1]	Hess et al. (2002)
Denmark	75	0.45	Jensen et al. (1993)
Borden 1 (fast)	2	0.08	Sudicky et al. (1983)
Borden 2 (slow)	11	0.16–0.32[1]	Gelhar et al. (1992)
Borden 3	86	0.5	Rajaram and Gelhar (1991)
Borden 4	25	0.3–0.8	Rivett et al. (1994)
Krauthausen	55	3.64[1]	Vereecken et al. (2000)
Wagna	312	18.3	Fank and Rock (2005)
Sued	234	30[1]	Boesel et al. (2000)
Horkheim	56.4	5.66[1]	Ptak and Teutsch (1994)
MADE	200	50–75[1]	Adams and Gelhar (1992)

[1]See explanation in text.

geometric mean of the dispersivities at about similar path length but having traveled along different trajectories. At *MADE*, the final dispersivity was based on the second moment reported by Adams and Gelhar (1992, 3303). The resulting 14 dispersivities in Table 3 cover a range of more than two orders of magnitude.

The parameters N and r are site specific so are the same for all experiments (cases) at a single site. The parameter r applies to cases with a path length larger than the length of domain A, that is, for $S > L_A$. For smaller path lengths, that is, $S < L_A$, only parameter N remains as an unknown. Therefore, parameter r will be derived after the assessment of N.

The scale factor N is the ratio between length and thickness of the conductivity zone and that of the averaging domain A as illustrated in Figure 2. For N in the range 0.1 to 0.5, the length of domain A, covering a single complete dispersion process, is 10 to 2 times the horizontal characteristic length λ_h (Table 2). Table 4 shows that dispersivities α_{calc} calculated for the above range of N sufficiently cover the range of the field values. The yellow cells contain values that fit best to the reported dispersivities α_{final}. The more heterogeneous the aquifer is, the wider the wake and the longer spread in Figure 3, top will be. Though the values of 0.3 and 0.4 seem close, the calculated dispersivities are sensitive to that difference, both in the initial and the repetition phase (Table 5). Therefore, the scale factor N is taken 0.4 for $\sigma_{\ln k}^2 < 1$ and 0.3 for $\sigma_{\ln k}^2 > 1$, which means that the length

of a single domain A is about five to seven times the characteristic length for weakly ($\sigma_{\ln k}^2 < 1$) respectively highly ($\sigma_{\ln k}^2 > 1$) heterogeneous aquifers (Table 2). This compares well with the width of the boundary zone in the infinite aquifer around the analytic element model of Jankovic et al. (2003).

The macroscale correlation coefficient r represents the degree of interdependency between dispersion in subsequent domains A. The range of r follows from statistic theory and is $0 \le r \le 1$. Table 5 shows the results using the values for N obtained above. The yellow cells show the selected values.

In weakly heterogeneous aquifers ($\sigma_{\ln k}^2 < 1$) and for relatively long travel distances ($S > L_A$), the value $r = 0$ fits best generating an equilibrium dispersivity (α_A). In heterogeneous aquifers ($\sigma_{\ln k}^2 > 1$) and for $S > L_A$, the value $r = 1$ fits best generating linear growth of the dispersivity with path length ($\alpha_S = \alpha_A * S/L_A$). The value of $r = 0.33$ for Twin Lakes 2 is explained in section Analysis of individual field experiments. In practice, the values $r = 0$ for $\sigma_{\ln k}^2 < 1$ and $r = 1$ for $\sigma_{\ln k}^2 > 1$ and an in-between value for r may be applied to analyze the process in the field.

Application to Field Experiments

Growth of Dispersivity with Travel Distance

The derived parameter values were applied in the analysis of the development of the dispersivity along the paths traveled in field experiments. Many of the selected experiments report series of data that enable to analyze the plume development over time. Table S.3.2 in File S3 describes the method of interpretation for each of the experiments. Dispersivities from the second moment of concentration distributions with travel distance were calculated using Equation 6 (Gelhar 1993, Chapter 5).

Using logarithmic scaling, Figure 5 shows the ratio of field over calculated dispersivities α_{Field} and α_{calc} versus the ratio of path length S over the site-specific length L_A of the averaging domain A. The latter ratio being smaller or larger than one distinguishes between the initial and repetition phase along the flowpath. Three types of assessment of dispersivity from field data are distinguished: (1) The method of second moments (Gelhar and Axness 1983), labeled 2M carried out for the experiments Borden 3, Cape Cod 1 and 2, Krauthausen and MADE. (2) The use of breakthrough curves (Ptak and Teutsch 1994), labeled BT applied to the experiments Twin Lakes, Denmark, Wagna, Sued, Horkheim. (3) The three-dimensional analytic method (Sudicky 1986), labeled 3A applied to the experiments Borden 1 and 2. Table 6 shows the statistics for the ratios of dispersivities for the 2M, BT, and 3A, and all types of data assessment.

The injection of a tracer at the origin of an experiment generates a concentration distribution that is not due to dispersion in water particles traveling in the aquifer. Freyberg (1986) presents a correction for

Table 4
Variation of the Calculated Dispersivity α_{calc} with Scale Factor N in the Initial Phase $S/L_A < 1$

	$\sigma^2_{\ln k}$	α_{final}	S/L_A	α_{cal}				
				$N = 0.5$	$N = 0.4$	$N = 0.3$	$N = 0.2$	$N = 0.1$
Twin Lakes 1	0.04	0.04–0.16	0.40	0.22	0.14	0.08	0.04	0.01
Borden 1	0.38	0.08	0.14	0.12	0.07	0.04	0.02	0
Borden 2	0.38	0.16–0.32	0.79	0.64	0.41	0.23	0.1	0.03
Sued	2.13	30	0.59	47.33	37.87	28.36	12.6	3.15
Horkheim	2.34	5.66	0.34	11.26	9.04	6.80	3.31	0.83

Selected values in yellow cells.

Table 5
Variation of the Calculated Dispersivity α_{calc} with Macroscale Correlation Factor r in the Repetition Phase $S/L_A > 1$

	$\sigma^2_{\ln k}$	α_{final}	S/L_A	N	α_{cal}		
					$r = 0$	$r = 0.33$	$r = 1$
Twin Lakes 2	0.04	0.55	2.66	0.4	0.35	0.55[1]	0.94
Cape Cod 1	0.24	0.96	5.42	0.4	0.94	4.75	10.24
Cape Cod 2	0.24	1.22	2.72	0.4	0.94	1.48	2.57
Denmark	0.37	0.45	12.00	0.4	0.45	2.10	5.35
Borden 3	0.38	0.5	3.21	0.4	0.52	1.40	3.19
Borden 4	0.38	0.3–0.8	1.79	0.4	0.52	0.65	0.93
Krauthausen	1.08	3.64	1.24	0.3	2.99	3.22	3.69
Wagna	1.08	18.3	4.25	0.3	4.14	8.59	17.61
MADE	7.00	50–75	2.44	0.3	30.29	36.79	47.31

Selected values in yellow cells.
[1]See Section "Application to Individual Field Experiments."

this by subtracting the variance of the concentration at the injection point from all forthcoming ones. The first reported variance was subtracted from the later ones for all 2M experiments. The experiment at Krauthausen will be discussed below. For BT and 3A experiments variances are not available. In these cases, extreme ratios of dispersivities in the first part of the initial phase, so just after the injection, were taken out, being one value in the series of the experiments *Twin Lakes 2*, *Borden 2* and *Wagna* as well as two values in the series of the experiment *Twin Lakes 1*.

Overall Results

The standard deviation of the ratio of dispersivities $\alpha_{Field}/\alpha_{calc}$ is larger (0.58 m) in the initial phase ($S/L_A < 1$) than that (0.24 m) in the repetition phase ($S/L_A > 1$). The plume spread caused by the flow through a single conductivity zone (Figure 3) can give considerable variation in the spread and the dispersivity in the initial phase. In the repetition phase, that is, at larger travel distances, the spread of the plume has grown such that the same local spread becomes relatively small. The standard deviation of the ratio of dispersivities for types BT and 3A (0.34 m) in the repetition phase varies more than that (0.24 m) for type 2M. The 2M method, which always covers a significant volume of solute, is less sensitive to the local variations of the tracer

concentration and/or the velocity. Overall in Figure 5 and Table 6, the agreement between field and calculated dispersivities is good, which opens deeper analysis of the experiments.

Application to Individual Field Experiments

In several field experiments, the observed dispersion can be better understood from the underlying advective transport phenomena.

- In the virtually homogeneous aquifer at *Twin Lakes*, the elongated shape of the conductivity zones (see λ_h in Table 2) may cause overlap along the flow path enabling fast particles to follow a chain of zones with relatively high conductivity. This well-known advective transport phenomenon causes strengthening of the growth of the plume front. This leads to interdependency of dispersion in the subsequent domains A in the repetition phase and supports the match of the dispersivities in Table 5 for $r = 0.33$.
- At *Cape Cod 2*, the dispersivity of 2.2 m reported (Hess et al. 2002) has been assessed from four observed plume shapes in the range $S/L_A = 1.7$ to 2.7 ($L_A = 40$ m), which is just beyond the initial phase. The reported variance and the final travel distance (Hess et al. 2002; Table 2) lead to $\Delta s = 16.3$ m and $\alpha_{final} = 1.22$ m (Table 3). These values compare well with the calculated values
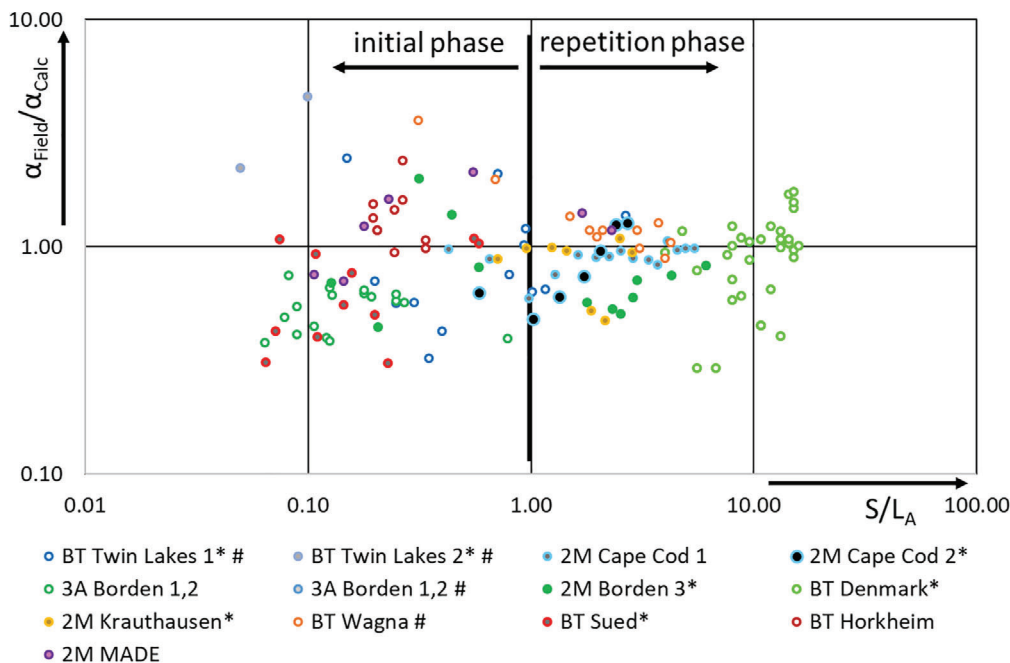
Figure 5. Ratio of field and calculated dispersivities versus ratio of path length S and L_A, the site-specific length of domain A. Abbreviations indicate the reported method of interpretation, where: 2M = second moment method; 3A = 3D Analytic Method; BT = Breakthrough curve fitting; # = omitted initial extreme values, see text; * = field experiment as discussed in the text.

of $\Delta s = 14.7$ m and $\alpha_{calc} = 0.94$ m (Table 3). (Hess et al. 2002) mention the presence of a high-conductivity layer. The local vertical movement of the plume into this layer as shown in Hess et al. (2002), Figure 3) causes the observed longitudinal spread so dispersivity to grow less than the calculated regional dispersivity. The velocity increase inside the high conductivity layer causes the increased local growth of the dispersivity. In the experiment Cape Cod 1 virtually along the same path but lower in the aquifer (Hess et al. 2002, Figure 6), this local advective transport phenomenon did not occur. It is concluded that the overall dispersivity of the aquifer is as in Table 3 and that the reported value of 2.2 m represents a local phenomenon.

- At *Denmark*, the experiment started with measurements taken far in the repetition phase. The significant variation around the equilibrium value of 1 in Figure 5 may come from the breakthrough curve interpretations, variations in the local velocities and/or variations in the effective porosity.

- In the experiment *Krauthausen*, the plume moved considerably downward into the base layer and beyond the reach of the observation network (Vereecken et al. 2000; Figure 9). The final reported stage is formed by remainders of high tracer concentration in low conductivity zones near the point of injection and low concentrations in the plume front. In all observed plume stages about 50% of the mass is recovered, which indicates that only half the volume of injection is transported in the observed part of the aquifer. Therefore, 50% of the first reported variance is used in the Freyberg (1986) correction.

Table 6
Number, Average, and Standard Deviation (Std Dev) for Groups of the Ratios $\alpha_{Field}/\alpha_{calc}$, Excluding Extreme Ratios Near Injection Point, See Text

Statistics on $\alpha_{Field}/\alpha_{calc}$		2M	BT-3A	All Types
Initial phase	N	20	49	69
$S < L_A$	Average	0.91	0.85	0.87
	Std Dev	0.58	0.53	0.55
Repetition	N	33	44	77
phase $S > L_A$	Average	0.86	0.99	0.93
	Std Dev	0.24	0.34	0.31
All	N	53	93	146
	Average	0.88	0.91	0.91
	Std Dev	0.40	0.46	0.43

Application to Spreading in Front and Tail

The distinctive calculation of values enables to analyze of the development the fronts and tails of plumes in the field. The growths of the spreads between two stages of each plume were assessed from figures that have been reported for 14 cases in 6 of the 9 experiments as specified in Table S.3.3 in File S3. The spread of each front and tail in the field is taken to be the distance in the flow direction between the center of the highest concentration and the contour-line of the lowest concentration. The growths in the spread Δs that result from this are shown in the columns field in Table 7, which should be read as an estimate rather than as an absolute value, because the interpolation underlying the reported

Table 7
Comparison of Growth of Various Spreads Δs, Calculated (Calc) and from Field Experiments (ΔS = path length between two plume stages; the colors of the numbers are explained in the text)

Case	ΔS (m) Path (m)	Δs_total (m) Field	Calc.	Δs_front (m) Field	Calc.	Δs_tail (m) Field	Calc.
Twin Lakes 1A	4	1.5	0.65	0.7	0.35	− 0.8	− 0.3
Twin Lakes 1B	7	5.5	1.2	2.5	0.6	− 3	− 0.6
Twin Lakes 2	20	6	3.4	3	1.55	− 3	− 1.85
Cape Cod 1A	100	40	33.1	15	11.4	− 25	− 21.9
Cape Cod 1B	200	50	49.7	20	17	− 30	− 32.8
Cape Cod 2	33	36	22.2	18	5.6	− 18	15.7
Denmark 1 Cl	24	16	13.3	6	4.8	− 10	− 8.5
Denmark 2 Tr	24	22	13.3	20	4.9	− 2	− 8.4
Borden 1	9.2	4.5	5.2	2.3	1.9	− 2.3	− 3.3
Borden 3A	44	28	13.6	14	5	− 14	− 8.6
Borden 3B	8	0.5	4.5	0.3	1.65	− 0.2	− 2.85
Borden 3C	54	19	15.1	6	5.5	− 13	− 9.6
Krauthausen	8	16	6.4	12	1.9	− 4	− 4.5
MADE 2	43	54	63.4	20	20.4	− 34	− 43

figures and the present assessment into numbers introduce uncertainties.

Clusters are identified in Table 7 by green color if the calculated and observed spreads differ less than two times by red if the difference is larger than four times and blue if in-between. The calculated and observed spreads match well for all path length between two plumes larger than 10 m, except at *Krauthausen* where the front spread in the field is about 10 times larger than the calculated spread. The agreement for the experiments *Twin Lakes 2*, *Cape Cod 1*, *Borden 1* and *3C* and *MADE* is even very good. In the cases where the path length between two plume stages is small, the observed development may be affected by a local conductivity zone. Such a zone may cause a local spread that is different from the spread calculated for the average process in the aquifer. The present comparison of field and calculated spreads is also an independent check of *N* and *r* because the difference between the front and the tail was not used before in the assessment.

In the experiment *Denmark 2*, the center of the tritium concentration apparently does not agree with the calculated one. This is opposite to the good fit of the chloride concentration in experiment *Denmark 1*. The front and the tail of the plume develop symmetrically in the experiments *Twin Lakes 2* and *Borden 1* and *3A* only. The calculated spreads of these experiments are slightly asymmetric, which comes from the difference in the thickness of the wakes of the front and tail as used in the length of distortion (Equation 4).

In conclusion: The methodology and the assessed parameter values do provide a consistent framework to better understand dispersion of plume fronts and tails in the field. The reader may verify his or her experiences with the spreadsheet that is provided in File S1.

So, What about the Three Main Issues Raised in the Introduction?

1. In some experiments the longitudinal dispersivity becomes constant with increasing pathlength and in other cases it remains growing.

In the initial phase in the first domain A, the dispersivity grows linearly with path length. In the repetition phase in weakly heterogenous aquifers, dispersion occurs independently in subsequent domains A and the dispersivity becomes constant. In heterogeneous aquifers, water particles may travel in subsequent high-conductivity zones. This generates interdependent dispersion in subsequent domains A and a linear and unlimited growth of the dispersivity with travel distance. This is strongly supported by the 146 dispersivities along the path in the selected field experiments. Unlimited growth of the longitudinal dispersivity with travel distance is not necessarily generated by unlimited increase of heterogeneity and aquifer dimensions underlying the unified scaling relations suggested by Neuman (1990).

2. Dispersivities reported from multiple comprehensive observations at a single site differ for similar pathlength, in some cases more than a factor 2.

The present methodology calculates dispersivities at the scale of the aquifer, which may differ from local values. Dispersivities from local gradients in the second moments of the tracer distribution may differ more than a factor two and originates in local conductivity zones. Dispersivities from breakthrough curves show similar magnitude differences but are more scattered, which is due to point-scale variation in the velocity as well as to the history of the individual path line.

3. The observed difference between the lengths of the front and the tail of a plume is not represented in the parameters reported from field experiments.

Most field experiments show asymmetric development of the front and the tail of a plume. This is not represented by the reported overall parameters longitudinal variance and dispersivity. The present methodology enables to calculate the distinct spread of the plume front and plume tail which proved to agree reasonably well with the observations in the experiments. An operational spreadsheet is available for the analysis of user defined situations. The parameter values derived for the different sites should give guidance for choosing input values.

Acknowledgments

Author's Note

The author does not have any conflicts of interest or disclosures to report.

Supporting Information

Additional supporting information may be found online in the Supporting Information section at the end of the article. Supporting Information is generally *not* peer reviewed.

File S1. User manual for the spreadsheet in supporting file S2.
File S2. This spreadsheet is the supporting file S1 to the paper in *Groundwater* entitled: Quantification of advective transport phenomena to better understand dispersion observed in the field, by W.J. de Lange.
File S3. Origin of data from references.

References

Adams, E.E., and L.W. Gelhar. 1992. Field study of dispersion in a heterogeneous aquifer 2 spatial moments analysis. *Water Resources Research* 28, no. 12: 3293–3307.

Appelo, C.A.J., and D. Postma. 1993. *Geochemistry*. Groundwater and Pollution. Rotterdam: A.A. Balkema.

Boesel, D., M. Herfort, T. Ptak, and G. Teutsch. 2000. Design, performance, evaluation and modeling of nature gradient multitracer transport experiments in a contaminated heterogeneous aquifer. In *Tracers and Modeling in Hydrogeology, Proceedings of the TraM'2000 Conference*. Vol. 262, ed. A. Dassargues, Brussels: IAHS, 45–51.

Dagan, G., and S.C. Lessoff. 2001. Solute transport in heterogeneous formations of bimodal conductivity distribution. 1. Theory. *Water Resources Research* 37, no. 3: 465–472.

Eames, I., and J.W.M. Bush. 1999. Longitudinal dispersion by bodies fixed in a potential flow. *Proceedings of the Royal Society A: Mathematical, Physical and Engineering Sciences* 455: 3665–3686.

Fank, J., and G. Rock. 2005. Tracer experiments on field scale for parameter estimation to calibrate numerical transport models. In *Reactive Transport in Soil and Groundwater*, ed. P. Viotti, G. Nützmann, and P. Asgaard, 11. Berlin, Heidelberg: Springer, 239–249.

Feehley, C.E., C. Zheng, and F.J. Molz. 2000. A dual-domain mass transfer approach for modeling solute transport in heterogeneous aquifers: Application to the macrodispersion experiment (MADE) site. *Water Resources Research* 36, no. 9: 2051–2515.

Fiori, A., G. Dagan, I. Jankovic, and A. Zarlenga. 2013. The plume spreading in the MADE transport experiment: Could it be predicted by stochastic models? *Water Resources Research* 49, no. 1: 2497–2507.

Fiori, A., I. Janković, and G. Dagan. 2006. Modeling flow and transport in highly heterogeneous three-dimensional aquifers: Ergodicity, gaussianity, and anomalous behavior—2. Approximate semianalytical solution. *Water Resources Research* 42. doi:10.1029/2005WR004752.

Fiori, A., A. Zarlenga, I. Jankovic, and G. Dagan. 2017. Solute transport in aquifers: The comeback of the advection dispersion equation and the first order approximation. *Advances in Water Resources* 110: 349–359.

Freyberg, D.L. 1986. A natural gradient experiment on solute transport in a sand aquifer, 2. Spatial moments and advection and dispersion of nonreactive tracers. *Water Resources Research* 22, no. 13: 2031–2046.

Garabedian, S.P., D.R. Leblanc, L.W. Gelhar, and M.A. Celia. 1992. Natural gradient tracer in sand and gravel Cape Cod, Massachusetts, 2. Analysis of spatial moment of non-reactive tracer. *Water Resources Research* 27, no. 5: 911–924.

Gelhar, L.W. 1993. *Stochastic Subsurface Hydrology*. Englewood Cliffs, New Jersey: Prentice Hall Inc.

Gelhar, L.W., and C.L. Axness. 1983. Three-dimensional stochastic analysis of macrodispersion in aquifer. *Water Resources Research* 19, no. 1: 161–180.

Gelhar, L.W., C. Welty, and K.R. Rehfeldt. 1992. A critical review of data on field-scale dispersion in aquifers. *Water Resources Research* 28, no. 7: 1955–1974.

Hess, K.M., J.A. Davis, D.B. Kent, and J.A. Coston. 2002. Multi-species reactive tracer test in an aquifer with spatially variable chemical conditions, Cape Cod, Massachusetts: Dispersive transport of bromide and nickel. *Water Resources Research* 38, no. 8: 36-1–36-17.

Jankovic, I., A. Fiori, and G. Dagan. 2003. Flow and transport in highly heterogeneous formations: 3. Numerical simulations and comparison with theoretical results. *Water Resources Research* 39, no. 9: 16-1–16-13.

Janković, I., A. Fiori, and G. Dagan. 2006. Modeling flow and transport in highly heterogeneous three-dimensional aquifers: Ergodicity, Gaussianity, and anomalous behavior—1. Conceptual issues and numerical simulations. *Water Resources Research* 42: 1–9.

Jensen, K.H., K. Bitsch, and P.L. Bjerg. 1993. Large-scale dispersion experiments in a Sandy aquifer in Denmark: Observed tracer movements and numerical analysis. *Water Resources Research* 29, no. 3: 673–696.

De Lange, W.J. 2020. Advective transport phenomena to better understand dispersion in field and modeling practice. *Groundwater* 58, no. 1: 46–55.

Lessoff, S.C., and G. Dagan. 2001. Solute transport in heterogeneous formations of bimodal conductivity distribution 2. Applications. *Water Resources Research* 37, no. 3: 473–480.

Moltyaner, G.L., and R.W.D. Killey. 1988. Twin Lake tracer tests: Longitudinal dispersion. *Water Resources Research* 24, no. 10: 1613–1627.

Moltyaner, G.L., M.H. Klukas, C.A. Wills, and R.D.W. Killey. 1993. Numerical simulations of Twin Lake atural gradient test, a comparison of method. *Water Resources Research* 29, no. 10: 3433–3452.

Neuman, S.P. 1990. Universal scaling of hydraulic conductivities and dispersivities in geological media. *Water Resources Research* 26, no. 8: 1749–1758.

Neuman, S.P., and D.M. Tartakovsky. 2009. Perspective on theories of non-Fickian transport in heterogeneous media. *Advances in Water Resources* 32, no. 5: 670–680.

Ptak, T., and G. Teutsch. 1994. Forced and natural gradient tracer tests in a highly heterogeneous porous aquifer, instrumentation and measurements. *Journal of Hydrology* 159: 79–104.

Rajaram, H., and L.W. Gelhar. 1991. Three-dimensional spatial moments analysis of Borden tracer test. *Water Resources Research* 27, no. 6: 1239–2482.

Rivett, M.O., S. Feenstra, and J.A. Cherry. 1994. Transport of a dissolved-phase plume from a residual solvent source in a sand aquifer. *Journal of Hydrology* 159: 27–41.

Sachs, L. 1984. *Angewandte Statistik*, 6th ed. Berlin, Heidelberg: Springer.

Schulze-Makuch, D. 2005. Longitudinal dispersivity data and implications for scaling behavior. *Groundwater* 43, no. 3: 443–456.

Strack, O.D.L. 1989. *Groundwater Mechanics*. New Jersey: Prentice Hall Inc.

Sudicky, E.A. 1986. Natural gradient experiment on solute transport in a sand aquifer: Spatial variability of hydraulic conductivity and its role in the dispersion process. *Water Resources Research* 22, no. 13: 2069–2082.

Sudicky, E.A., J.A. Cherry, and E.O. Frind. 1983. Migration of contaminants in groundwater at a landfill. A case study: 4. A natural gradient dispersion test. *Journal of Hydrology* 63: 81–108.

Vereecken, H., U. Doring, H. Hardellauf, U. Jaekel, U. Hashagen, O. Neuendorf, H. Schwarze, and R. Seideman. 2000. Analysis of solute transport in a heterogenous aquifer: The Krauthausen field experiment. *Journal of Contaminant Hydrology* 45: 329–358.

Zech, A., S. Attinger, V. Cvetkovic, G. Dagan, P. Dietrich, A. Fiori, Y. Rubin, and G. Teutsch. 2015. Is unique scaling of aquifer macrodispersivity supported by field data? *Water Resources Research* 51: 7662–7679.